Optics Communications 574 (2025) 131150

Contents lists available at ScienceDirect

Optics Communications

journal homepage: www.elsevier.com/locate/optcom

Efficient single-mode operation in a 10 dB/m absorption very-large-mode-area ytterbium-doped optical fiber via curvature-induced mode filtering

Tristan Guezennec [a], Laurent Provino [a], David Landais [a,1], Achille Monteville [a], Olivier Le Goffic [a], Robin Pouyet [a], Bertrand Dudoux [a], Thierry Chartier [b], Adil Haboucha [a,*]

[a] Photonics Bretagne, 4 rue Louis de Broglie, 22300, Lannion, France
[b] Institut FOTON, CNRS UMR 6082, 6 rue de Kerampont, 22300, Lannion, France

ARTICLE INFO

Keywords:
Yb-doped fiber
High power fiber amplifier
Very large modal area
Single-mode fiber
Polarization maintaining fiber
All-solid fiber

ABSTRACT

In this paper we report our findings on the design, manufacturing and testing of low numerical aperture active step-index optical fibers with very large mode area, operating in a truly single-mode regime. Our approach to efficiently filter higher-order modes in the core relies on applying curvature in a specific direction at a given diameter on a specially designed fiber containing boron-doped silica rods on both sides of the core. The fabricated ytterbium-doped fibers exhibit a mode field diameter of 32 μm, a cladding pump absorption of 10 dB/m and were designed for use in a compact monolithic configuration due to its all-solid nature and its 14 cm targeted bend diameter.

1. Introduction

The last decade has seen the rapid development of high peak power fiber amplifier, which has been enabled by the development of large mode area (LMA) fiber amplifiers. This ever increasing quest for large effective area is essentially driven by the necessity to mitigate the non-linear effects which can lead to detrimental pulse distortions. In addition, most applications high peak power require polarization maintaining fiber architecture further complicating preform and fiber fabrication processes. Unfortunately state-of-the-art rare-earth (RE) doped conventional manufacturing process limitations have prevented the development of truly single-mode RE doped fibers with core diameters greater than 20 μm at 1 μm [1]. Equally important is the need for offering high beam quality and excellent pointing stability. As the core diameter of LMA fibers is increased to beyond ~15 μm, manufacturing single-mode fibers becomes difficult with sufficient yield due to the required index precision obtainable even with state-of-the-art rare-earth-doped core manufacturing processes (typ. 1×10^{-4}). To circumvent this limitation, different VLMA fiber designs involving microstructuration have been proposed over the past ten years, such as photonic crystal fibers (PCF) [2], leakage channel fibers [3], or solid-core photonic bandgap fiber [4]. But all these fibers extremely are difficult to fabricate due to their stringent requirement on the refractive indexes for core and cladding which must be the same. To date, VLMA PCFs remain the only commercially viable way to achieve large mode-field diameters (MFD). However, their complex design requires intricate splicing and packaging solutions, which often limit or prevent monolithic integration. Additionally, their large coil diameter and incompatibilities with fused-fiber components constrain their compactness, forcing laser developers to make trade-offs between performance and practicality.

Alternative approaches have deviated from the traditional robust single-mode operation used in PCFs, that is making the fiber nearly or strictly single-mode by introducing losses or delocalizing higher-order modes (HOMs). A key aspect of these fibers is that they rely on manufacturing-friendly step-index core designs with a very low numerical aperture (NA) between 0.030 and 0.045 [5–7]. For example, output powers of up to 3 kW at 1064 nm and a laser efficiency of approximately 90% with 50 μm-core diameter and a 0.030 NA in a step-index Yb double-clad fiber have been demonstrated [5]. Despite the good performances achieved in these implementations, these fiber designs present certain limitations. None of these fibers are truly polarization maintaining (PM), which complicates practical integration or the development of lasers. Moreover, the single-mode operation achieved through an extremely low index contrast of the core requires stricter bending over larger diameters and a higher sensitivity to bend-induced losses for the fundamental modes.

* Corresponding author.
E-mail address: ahaboucha@photonics-bretagne.com (A. Haboucha).
[1] Currently at Lumibird, Lannion, France.

https://doi.org/10.1016/j.optcom.2024.131150
Received 15 July 2024; Received in revised form 18 September 2024; Accepted 23 September 2024
Available online 27 September 2024

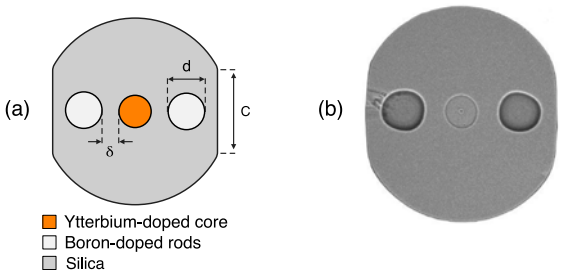

Fig. 1. (a) Schematic representation of the fiber design (δ: the edge-to-edge distance between the core and the boron-doped rod, d: the boron-doped rods diameter, C: length of the flat surfaces). (b) SEM picture of the fabricated fiber after stripping the low-index polymer outer cladding (the core and boron-doped silica rods were revealed by hydrofluoric acid etching).

In this paper, we present a new all-solid step-index PM double clad VLMA fiber providing similar effective area than state-of-the-art commercial fibers, robust suppression of HOMs and immunity to signal bend loss. These were from engineering of the core's refractive index difference and the stress applying parts (SAPs). The resulting fiber was drawn at Photonics Bretagne facilities and implemented in a monolithic laser system based on fused-fiber commercial components.

2. Design and simulations

The design of the fiber is the one reported on Fig. 1(a). It consists of a 40 µm diameter Yb-doped core, surrounded by two boron-doped silica rods ensuring a targeted 1×10^{-4} phase birefringence. The cladding geometry is circular based with two opposite flat surfaces perpendicular to the boron-doped silica rods alignment allowing both a better pump scrambling and a preferential bending direction, for a purpose that we will develop later.

The designing steps are the following:

2.1. Core diameter

From a given preform refractive index profile, we perform a series of finite element method (FEM) computation in order to define the core diameter that will allow a MFD of 32 µm, while keeping the fundamental mode losses to a reasonable level.

2.2. Cladding geometry

In order to achieve a 10 dB/m cladding pump absorption, the cladding must follow:

$$A_{Clad} = \frac{\alpha_{Abs}^{Core}}{\alpha_{Abs}^{Clad}} \times A_{Core} \tag{1}$$

with A_{core} and A_{clad} the core and cladding areas, and α_{Abs}^{Core} and α_{Abs}^{Clad} the core and cladding pump absorptions. We evaluate the core absorption (at 976 nm wavelength) at 300 dB/m using fluorescence under 976 nm radiation excitation. According to this condition, we found that a 220 µm clad diameter (D_{clad}) allows a 10 dB/m cladding pump absorption.

2.3. Stress applying parts

The next part to be dimensioned are the SAPs. These can be defined by two parameters, namely the boron-doped rods diameter d and the edge-to-edge distance between the core and the boron-doped rod δ. A set of computations is done in order to find the couples (d, δ) that gives a phase birefringence level of 1×10^{-4} at the 1064 nm wavelength. Here the phase birefringence has been estimated according to the following relation for typical 18 % mol boron doped stress rods [8]:

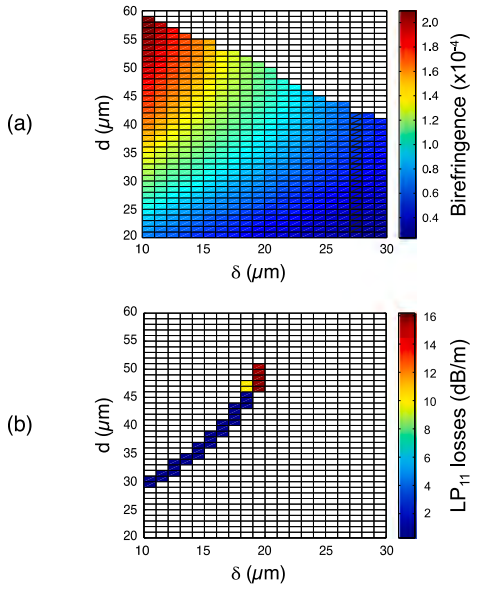

Fig. 2. (a) Simulated birefringence according to the SAPs parameters. (b) Simulated LP_{11} losses according to the SAPs parameters for a 14 cm bend diameter. All simulations were performed at the wavelength of 1064 nm.

$$B = \frac{2EC}{1-\nu} \Delta\alpha \left(T - T_{ref}\right) \left(\frac{d}{2d_{core/SAP}}\right) \left[1 - 3\left(\frac{2d_{core/SAP}}{D_{clad}}\right)^4\right] \tag{2}$$

$$d_{core/SAP} = \delta + \frac{d + d_{core}}{2} \tag{3}$$

with E representing Young's modulus, ν Poisson's ratio, C the stress-optic coefficient, $\Delta\alpha$ the thermal expansion coefficient difference between boron-doped silica and pure silica, T the high temperature, T_{ref} the reference temperature (e.g., room temperature), d_{core} the core diameter and $d_{core/SAP}$ the center-to-center distance between the core and the stress rods.

Once these values are identified, we perform another set of computation in order to evaluate the LP_{11} mode losses (least lossy HOM) for a given bending diameter, here 14 cm, and search for the values that exhibits losses above 10 dB/m. The simulations were carried out using a finite element method, taking into account the stress fields induced by the boron-doped rods on the refractive index of the fiber's 2D profile. The modal losses were estimated by adding an APML (Absorbing Perfectly Matched Layer) around the structure. As depicted in Fig. 2(b), these conditions allow only a few values for d and δ.

We then initially performed a series of simulations to estimate losses of the LP_{01} fundamental modes and first four high order modes LP_{11} in relation to the bending diameter, for two bending direction: one parallel to the slow axis, given by the SAPs alignment, and one perpendicular to this axis. The parameters d and δ chosen from the previously selected solutions for these simulations are, respectively, 46 µm and 19 µm. In addition a draw induced index change of $+1.5 \times 10^{-4}$ corresponding to about 50 grams draw tension for a 220 µm fiber diameter was taken into account in the simulations to reflect the fiber core/clad index difference.

These computations show that in order to be truly single-mode with minimum losses for the fundamental mode, this fiber must be to be coiled with a 14 cm diameter along the slow axis, thereby insuring a LP_{11} loss level above 10 dB/m. As depicted in Figs. 3 (a) and (b), we observe that the fiber exhibits high losses for the fundamental modes when coiled along the fast axis, so the opposites flat sides are here to ensure that the fiber will be coiled along its slow axis. This observation

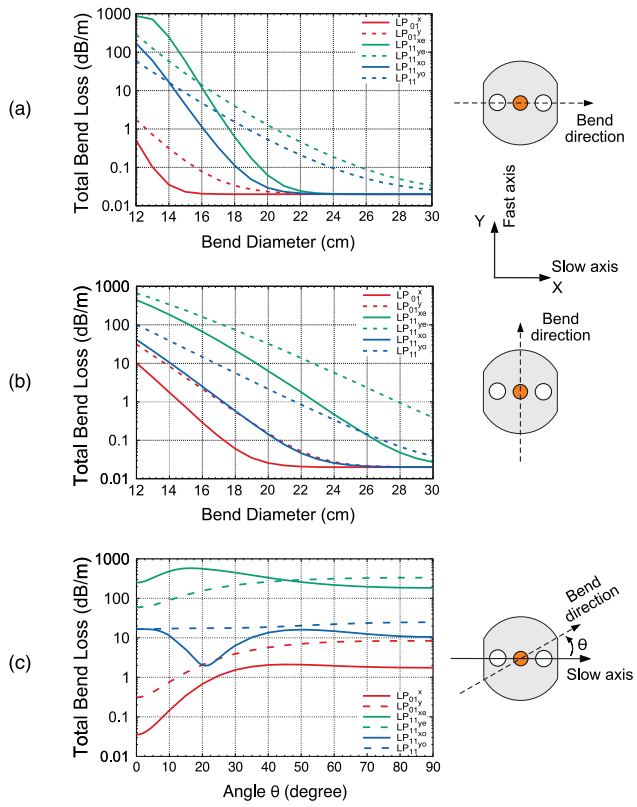

Fig. 3. (a) Simulated losses in regard of the bending diameter for a coil direction parallel to the slow axis. (b) Simulated losses in regard of the bending diameter for a coil direction perpendicular to the slow axis. (c) Simulated losses in regard of the bending angle related to slow axis.

can be explained by the mechanical stresses induced by the boron-doped rods positioned symmetrically on either side of the core. These rods generate localized stress fields that slightly increase the refractive index in the regions between the core and the rods along the slow axis, thereby confining the electromagnetic field. In contrast, along the fast axis, the refractive index of the silica is lower, allowing more field leakage. When the fiber is bent in the plane corresponding to the fast axis, the electromagnetic field can expand more freely because the boron-doped rods do not block the field expansion in this direction. This unconfined expansion, combined with the lower refractive index in the fast axis direction, results in greater susceptibility to bending losses for the fundamental mode. This is exacerbated by the low numerical aperture of the core, which further promotes field leakage. To mitigate this, the fiber is designed with flats, which guide the bending along the slow axis, ensuring better confinement and lower losses for the fundamental mode polarized along the slow axis.

Finally, we examined how the angular misalignment of the bending direction relative to the stress rods affects the guided mode losses. To do this, we simulated the total losses of the LP_{01} and LP_{11} modes as a function of the bending angle θ relative to the slow axis, with a bending diameter of 14 cm. Our simulation results, shown in Fig. 3(c), indicate that for an angular misalignment lower than 10°, the losses of the LP_{01} mode polarized along the slow axis remain below 0.1 dB/m. However, for greater angular misalignment, the losses increase significantly, and the condition of low losses for this fundamental mode can no longer be met, making the fiber unsuitable for practical use in fiber amplifiers or fiber lasers. We also note that for an angular misalignment around 20°, the higher-order mode $LP_{01}{}^{xo}$ exhibits lower losses of about 2 dB/m, similar to the fundamental mode polarized along the fast axis.

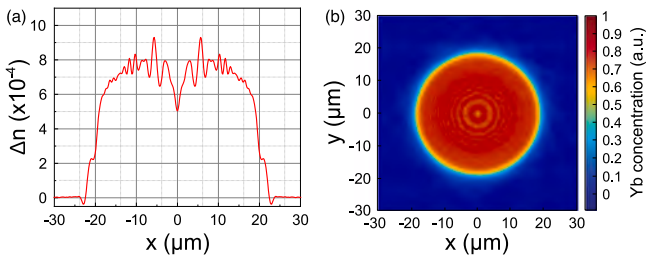

Fig. 4. (a) Refractive index profile of the core measured using an interferometric fiber analysis system. (b) 2D Yb-doping profile measured under 976 nm radiation excitation.

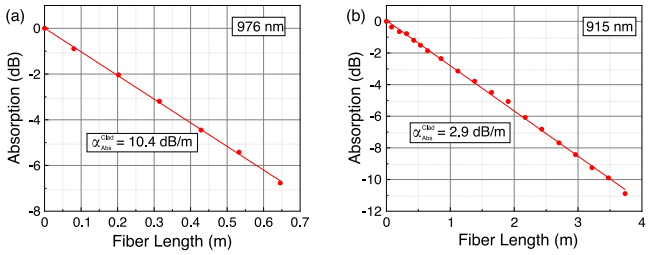

Fig. 5. Cladding pump absorption measurements at (a) 976 nm wavelength and (b) 915 nm wavelength, using a cut-back method. Red dots are the experimental data and the red lines are linear fits.

3. Fabrication & characterization

The core preform has been manufactured using a modified chemical vapor deposition method, along with chelate precursors. The core consist of a Al_2O_3/P_2O_5 matrix with approximately equivalent doping in order to decrease the photodarkening effects [9]. The boron-doped silica rods were incorporated into the preform via drilled holes in the preform. The fiber was draw in a low-index polymer coating providing a cladding aperture of about 0.46. The drawing tension was carefully controlled to minimize variations in the refractive index of the ytterbium-doped core and deformations of the flat surfaces. An SEM picture of end-face of the fabricated fiber is shown in Fig. 1(b). The geometric parameters estimated from the SEM picture analysis are very close to the target values: average core diameter around 40 μm, average diameter of the stress rods around 46 μm, spacing between the stress rods and the core around 19 μm, and the internal cladding diameters of 224 μm for the major axis and 208 μm for the minor axis.

The refractive index profile of the fabricated fiber was measured using an interferometric fiber analysis system. The effective refractive index, as depicted in Fig. 4, was measured to be 7.0×10^{-4}, resulting in a numerical aperture of 0.045. As previously mentioned, the Yb-doping profile was measured using fluorescence under 976 nm excitation, revealing a uniform profile as represented in Fig. 4(b). The small-signal cladding pump absorption has been measured using a cut-back method with a broadband light source. Because of the strong absorption at 976 nm pump wavelength, we were able to perform this measurement with a limited length of fiber, from 10 cm to 70 cm. In the mean time, we were able to measure the cladding absorption for 915 nm pump radiation within a 4 m long fiber. We obtained a pump absorption of 10.4 dB/m and 2.9 dB/m at 976 nm and 915 nm wavelengths respectively, as presented in Fig. 5.

In the end, we measured the phase birefringence of the fabricated fiber. We used a Faraday magneto-optic based setup to measure the beat length at 1064 nm with a similar setup as in [10]. A 1064 nm linearly polarized laser diode is launched in the fiber, and the transmitted intensity is measured while a coil is moving along the fiber, creating a magnetic field. The recorded output changes with a periodic value linked to the beat length. In order to clearly identify the beat length,

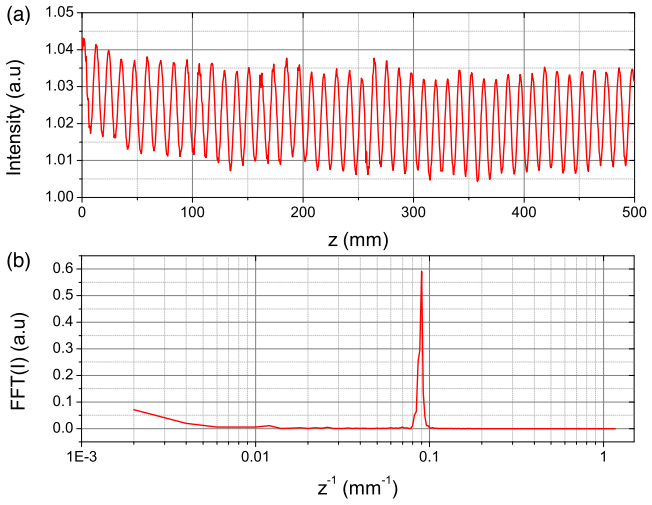

Fig. 6. Phase birefringence measurements. (a) Intensity recording at the output of the fiber in regard of the coil position. (b) Fourier transform of the intensity.

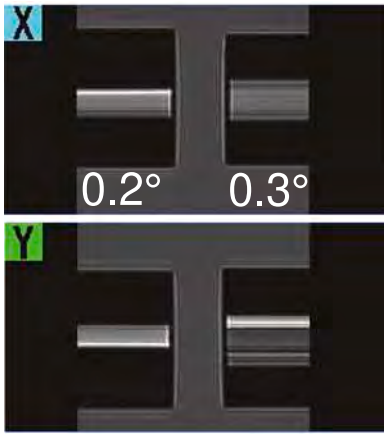

Fig. 7. Typical cleave results with a standard large diameter fiber cleaver, shown from both front and back views.

and to ensure that there is no intermodal interferences, we computed the Fourier transform of the measured intensity, as depicted in Fig. 6. The measured beat length is 11.11 mm ± 0.24 mm, giving a phase birefringence of $9.6 \times 10^{-5} \pm 3 \times 10^{-6}$, which is sufficiently close to the targeted value.

4. Integration & laser testing

Due to its all-solid design, the fiber can be easily cleaved using a standard large-diameter fiber cleaver and spliced without requiring any polishing step. However, in our case, we encountered a specific challenge: during fiber positioning in the inserts, the flat sections on the stripped side of the fiber caused slight twisting when clamped in the cleaver, which affected the cleaving quality. To address this issue, we implemented a simple protocol that ensures no twisting of the fiber during the cleaving process. This method has proven to be highly repeatable. For example, out of 16 cleaves, we consistently achieved an average cleave angle of 0.3° with a standard deviation of 0.15°. Moreover, as shown in Fig. 7, this approach allowed us to achieve a typical sub−0.5° cleave angle, demonstrating both precision and repeatability.

In order to seamlessly integrate our fiber into a monolithic configuration, it needs to be spliced with standard commercial fibers. To achieve this, we developed a custom Mode-Field Adapter (MFA) based

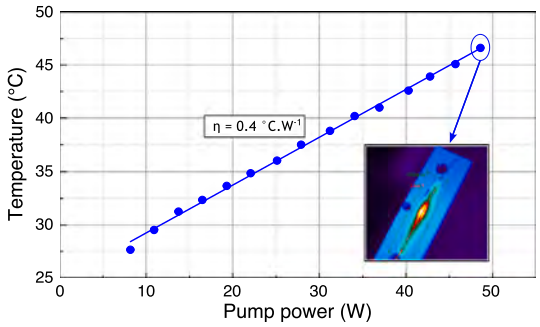

Fig. 8. MFA temperature in regard to pump power. The blue dots are the experimental data and the blue line is a linear fit. Inset: thermal image of the MFA for the maximum pump power.

on multimode self-imaging graded index (GRIN) fibers [11]. The MFA consists an 800 μm long GRIN fiber, meticulously drawn in our laboratory, capable of accommodating Mode-Field Diameter (MFD) variations from ~11 μm to 32 μm. This ensures optimal mode adaptation between our fiber and a standard 11/125 PM double-clad passive fiber with 0.08 core NA. Following the splice, the MFA is coated with a low refractive index polymer and housed in aluminum casing to facilitate passive thermal dissipation, a crucial consideration as the MFA also manages the co-propagating 60 W pump power in our laser setup.

The 4-meter-long fiber is mounted and coiled with a bending diameter of 14 cm for three loops on a 10 mm thick aluminum plate. One end of the fiber is left loose. The coiling of the fiber was facilitated by grooving a spiral of the nominal diameter on the aluminum plate, in accordance with our simulation results. Thermal paste was applied along the fiber to improve heat dissipation, although it was not strictly necessary given the power levels involved in this experiment. However, its use could become essential when the fiber is implemented in systems with significantly higher power levels. While positioning the fiber in the groove, we did not encounter any difficulty in orienting the fiber curvature along the alignment axis of the boron-doped silica rods. Before positioning the fiber on the aluminum plate, we first checked that the fiber aligned naturally in the transverse plane of the two flat surfaces, with a length C estimated around 90 μm on the manufactured fiber (see Fig. 1(a)). Despite the circular shape of the fiber with the addition of the low-index polymer double cladding, we explain the fiber's preferential orientation by the difference in stiffness between the claddings, due to their significant thickness differences (50 μm for the second outer low-index polymer cladding and 220 μm for the inner silica cladding), as well as the large difference in modulus of elasticity between silica (7.25×10^4 N/mm^2 at 20 °C) and the polymer (between 20 N/mm^2 and 500 N/mm^2 at 20 °C).

Fig. 8 illustrates that with passive cooling, the MFA exhibits a heat load of 0.4 ° C/W from room temperature, ensuring the MFA remains at a manageable temperature. Importantly, the heat load is evenly distributed across the MFA, preventing the formation of localized hot spots. Additionally, during the handling and mounting of the fiber, we took special care to minimize mechanical stress and ensure stable operation of the fiber laser system. The fiber was securely mounted on the aluminum plate, with precautions taken to avoid excessive bending or tension that could degrade its performance.

To evaluate the mode adaptation between the Yb-doped fiber and standard commercial fiber, we conducted experimental tests measuring mode profiles, coupling efficiencies, and transmission properties to validate the Mode Field Adapter (MFA). A test bench was developed to integrate the MFA onto the VLMA active fiber, using:

- A polarized SLED source (CWL = 1050 nm, 70 nm 3 dB bandwidth),
- A splicing station to connect the input fiber to the VLMA fiber,

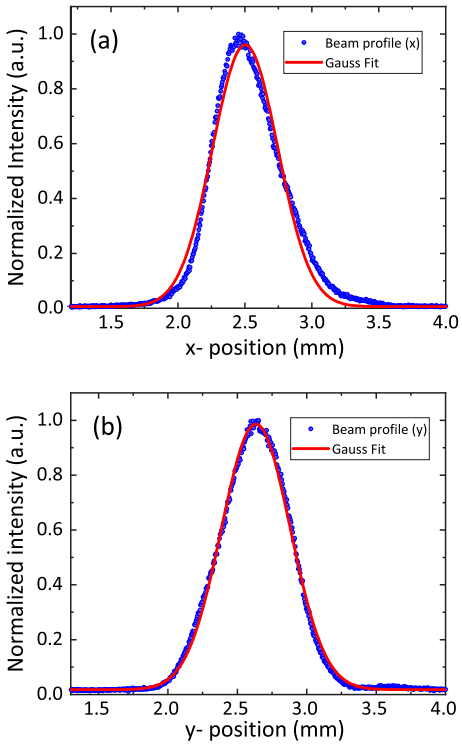

Fig. 9. Gaussian fit (red curve) of the experimental beam intensity profile (blue) after the MFA in the (a) x-and (b) *y*-directions.

- A system to monitor output power, mode profile, and Polarization Extinction Ratio (PER).

This setup optimized the MFA's performance, but signal absorption in the Yb-doped core prevented precise insertion loss (IL) measurements. Additional tests on a passive version of the VLMA fiber, with similar properties but no absorption, provided a more accurate IL of ~0.4 dB ± 0.1 dB. The beam exiting the MFA was collimated and directed towards the Spiricon SP620U camera-based beam profiler system. Transverse cuts of the far-field spatial profile in both the x- and *y*-directions were plotted and are shown in Fig. 9.

The fiber was implemented in a fiber chirped pulse amplification (FCPA) system, delivering a 100 mW, 20 MHz pulse train with 400 ps, 1040 nm pulses, as described in [12]. When the optical beam exits the booster stage (Yb-doped VLMA fiber), undesirable effects like parasitic reflections can reduce amplification gain, and uncontrolled high-power signal pulses can be re-injected, potentially damaging the amplification stages and their pumps.

To enhance system reliability during power scaling, an appropriate termination was implemented to ensure high isolation. In our setup, the output end of the active fiber was terminated with a 2 mm long F300 glass end cap, beveled at 4° to provide enhanced isolation. As the beam passes through the glass end cap, it diverges, reducing its density at the glass–air interface and preventing damage to the glass. An image of the end cap is shown in Fig. 10.

The residual pump is typically removed by integrating a cladding mode stripper before the end cap. However, in our case, to accurately evaluate the fiber's performance, we needed access to the residual pump for measurement. The output beam was first collimated using an aspheric lens, then directed to a dichroic mirror to separate the amplified signal from the residual pump. The signal was further distributed to different diagnostic branches via wedges and mirrors, enabling simultaneous measurements of amplification efficiency, spectro-temporal characteristics, beam profile, and spatial quality of the output signal.

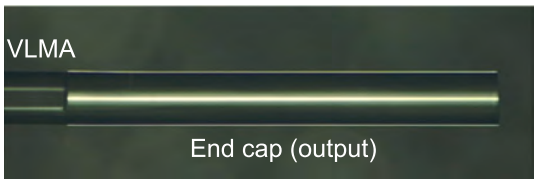

Fig. 10. Optical microscope image of the all-fiber end cap at the output of the booster stage.

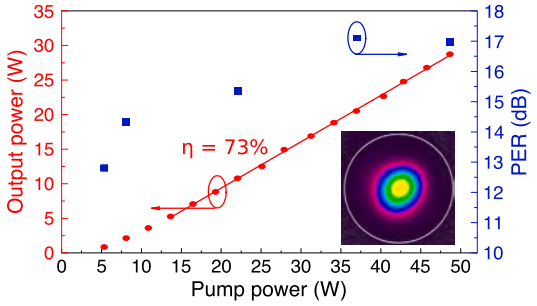

Fig. 11. Output power (red color) and PER (blue color) versus pump power. Red and blue dots are the experimental data and the red solid line is a linear fit. Inset: Typical output beam profile.

The experimental results obtained from the fiber laser system demonstrated exceptional performance characteristics. As depicted in Fig. 11, the observed amplification efficiency surpassed expectations, while the polarization extinction ratio exceeded 17 dB, indicating robust polarization maintenance.

To characterize the spatial profile at the fiber output under amplification conditions, we performed a beam quality measurement using Ophir's BeamSquared SP204S M^2 Measurement System. We obtained values of 1.12 and 1.18 in the two axes, which is very acceptable for this new fiber. We did not observe any indication of the fiber behaving in a non-single-mode behavior. The fact that the M^2 value slightly exceeds 1.1 can be explained by the mode being slightly elliptical, which is inherent to the design of this fiber.

These results, highlight the suitability of our fiber for demanding applications such as high-power laser machining.

5. Conclusion

We successfully demonstrate that accurate definition and optimization of core refractive index along with SAPs geometrical parameters allows standard double-clad step index fibers to reach high effective areas, while keeping a single-mode operation. The fabricated fiber was implemented in a monolithic fiber system, displaying a significant advancement in the field of high-power fiber optics by providing a versatile and reliable solution for monolithic laser architectures. The combination of innovative design, meticulous fabrication and thorough characterization has paved the way for practical implementation of our fiber in various industrial and scientific settings.

Fundings

This work was caried out in the framework of the 4F project (French laser Fibers for Factories of the Future), funded by BPI France, and the LAGRIF project (Laser for the Agriculture of the Future), funded by FEDER, grant number 1110/EU001051/00065007 and Région Bretagne, France

CRediT authorship contribution statement

Tristan Guezennec: Writing – original draft, Visualization, Investigation. **Laurent Provino:** Writing – review & editing, Visualization, Software, Methodology, Conceptualization. **David Landais:** Resources, Investigation. **Achille Monteville:** Resources, Investigation. **Olivier Le Goffic:** Resources, Investigation. **Robin Pouyet:** Writing – review & editing, Resources, Investigation. **Bertrand Dudoux:** Writing – review & editing, Resources. **Thierry Chartier:** Resources, Investigation. **Adil Haboucha:** Writing – review & editing, Validation, Resources, Investigation.

Declaration of competing interest

Laurent Provino holds several pending patents filed by Photonics Bretagne: #US20240097396A1, #JP2024501614A, #EP4002608A1, and #CA3198595A1. The other authors declare no known competing financial interests or personal relationships that could have influenced the work reported in this paper.

Data availability

Data will be made available on request.

References

[1] M.-J. Li, X. Chen, A. Liu, S. Gray, J. Wang, D.T. Walton, L.A. Zenteno, Limit of effective area for single-mode operation in step-index large mode area laser fibers, J. Lightwave Technol. 27 (15) (2009) 3010–3016, http://dx.doi.org/10.1109/JLT.2009.2020682.

[2] T.T. Alkeskjold, M. Laurila, L. Scolari, J. Broeng, Single-mode ytterbium-doped large-mode-area photonic bandgap rod fiber amplifier, Opt. Express 19 (8) (2011) 7398–7409, http://dx.doi.org/10.1364/OE.19.007398.

[3] F. Kong, G. Gu, T.W. Hawkins, J. Parsons, M. Jones, C. Dunn, M.T. Kalichevsky-Dong, K. Wei, B. Samson, L. Dong, Flat-top beam from a 50 μm-core Yb-doped leakage channel fiber, in: Optical Fiber Communication Conference, Optica Publishing Group, 2014, p. Tu3K.5, http://dx.doi.org/10.1364/OFC.2014.Tu3K.5.

[4] S.R. Petersen, T.T. Alkeskjold, F. Poli, E. Coscelli, M.M. Jørgensen, M. Laurila, J. Lægsgaard, J. Broeng, Hybrid Ytterbium-doped large-mode-area photonic crystal fiber amplifier for long wavelengths, Opt. Express 20 (6) (2012) 6010–6020, http://dx.doi.org/10.1364/OE.20.006010.

[5] V. Petit, R.P. Tumminelli, J.D. Minelly, V. Khitrov, Extremely low NA Yb doped preforms (<0.03) fabricated by MCVD, in: J. Ballato (Ed.), in: Fiber Lasers XIII: Technology, Systems, and Applications, vol. 9728, International Society for Optics and Photonics, SPIE, 2016, p. 97282R, http://dx.doi.org/10.1117/12.2214546.

[6] D. Jain, Y. Jung, P. Barua, S. Alam, J.K. Sahu, Demonstration of ultra-low NA rare-earth doped step index fiber for applications in high power fiber lasers, Opt. Express 23 (6) (2015) 7407–7415, http://dx.doi.org/10.1364/OE.23.007407.

[7] F. Beier, C. Hupel, J. Nold, S. Kuhn, S. Hein, J. Ihring, B. Sattler, N. Haarlammert, T. Schreiber, R. Eberhardt, A. Tünnermann, Narrow linewidth, single mode 3 kW average power from a directly diode pumped ytterbium- doped low NA fiber amplifier, Opt. Express 24 (6) (2016) 6011–6020, http://dx.doi.org/10.1364/OE.24.006011.

[8] P.L. Chu, R.A. Sammut, Analytical method for calculation of stresses and material birefringence in polarization-maintaining optical fiber, J. Lightwave Technol. 2 (5) (1984) 650–662, http://dx.doi.org/10.1109/JLT.1984.1073673.

[9] M. Likhachev, S. Aleshkina, A. Shubin, M. Bubnov, E. Dianov, D. Lipatov, A. Guryanov, Large-mode-area highly Yb-doped photodarkening-free Al_2O_3-P_2O_5-SiO_2-based fiber, 2011, http://dx.doi.org/10.1109/CLEOE.2011.5943202.

[10] T. Chartier, C. Greverie, L. Selle, L. Carlus, G. Bouquet, L.-A. de Montmorillon, Measurement of the stress-optic coefficient of single-mode fibers using a magneto-optic method, Opt. Express 11 (20) (2003) 2561–2566, http://dx.doi.org/10.1364/OE.11.002561.

[11] G.P. Agrawal, Invite paper: Self-imaging in multimode graded-index fibers and its impact on the nonlinear phenomena, Opt. Fiber Technol., Mater. Devices Syst. 50 (2019) 309–316, http://dx.doi.org/10.1016/j.yofte.2019.04.012.

[12] T. Guezennec, L. Provino, E. Lallier, O.L. Goffic, D. Landais, A. Monteville, T. Taunay, A. Haboucha, Sub-500 fs high power quasimonolithic FCPA laser using an all-solid step-index flexible PM VLMA Yb-doped fiber amplifier, in: Micro-Structured and Specialty Optical Fibres VII, vol. 12140, International Society for Optics and Photonics, SPIE, 2022, 1214007, http://dx.doi.org/10.1117/12.2624096.